Surface & Coatings Technology 221 (2013) 182–190

Contents lists available at SciVerse ScienceDirect

Surface & Coatings Technology

journal homepage: www.elsevier.com/locate/surfcoat

Novel performance in physical and corrosion resistance HfN/VN coating system

C. Escobar [a], M. Villarreal [a], J.C. Caicedo [b,*], W. Aperador [c], P. Prieto [a,d]

[a] Thin Film Group, Universidad del Valle, A.A. 25360, Cali, Colombia
[b] Tribology Polymers, Powder Metallurgy and Processing of Solid Waste Research Group Universidad del Valle, Cali, Colombia
[c] Ingeniería Mecatrónica, Universidad Militar Nueva Granada, Bogotá, Colombia
[d] Center of Excellence for Novel Materials, CENM, Cali, Colombia

ARTICLE INFO

Article history:
Received 27 July 2012
Accepted in revised form 5 February 2013
Available online 19 February 2013

Keywords:
Electrochemical properties
Multilayered systems
Protective coatings

ABSTRACT

4140 steel substrates were coated with hafnium nitride/vanadium nitride multilayered with the objective of improving their corrosion resistance. The multilayered coatings were grown via a reactive r.f. magnetron sputtering technique by systematically varying the bilayer period (Λ) and the bilayer number (n) while maintaining constant the total coating thickness (~1.2 μm). The coatings were characterized by X-ray diffraction (XRD), electron and transmission microscopy. The electrochemical properties were studied by Electrochemical Impedance Spectroscopy and Tafel curves. XRD results showed preferential growth in the face-centered cubic (111) crystal structure for $[HfN/VN]_n$ multilayered coatings. The best enhancement of the mechanical behavior was obtained when the bilayer period (Λ) 15 nm (n = 80) which yielded the highest hardness (37 GPa) and elastic modulus (351 GPa). The values for the hardness and elastic modulus are: 1.48 and 1.32 times greater than the coating with n = 1, respectively. The maximum corrosion resistance was obtained for coatings with (Λ) equal to 15 nm, corresponding to bilayer n = 80. Polarization resistance and corrosion rate was around 112.19 kΩ cm^2 and $0.094*10^{-3}$ mmy respectively, these values were 172.6 and 0.007 times better than those shown by the uncoated 4140 steel substrate (0.65 kΩ cm^2 and 0.014 mmy, respectively).

1. Introduction

The nitride materials used under physical methods on cutting or that have shown corrosive or mechanical applications exhibit favorable results. Among the different methods reactive magnetron sputtering has proven quite successful [1]. Considering this, at present it is possible to find a broad variety of hard coatings tested and used in industries, along with several substrate materials [2]. Previous studies have reported that the concept of multilayers offers a potent solution for chemical properties in hard coatings. Coatings deposited via physical vapor deposition (PVD) based on nitrides (HfN [3], VN [4] and TiCN [5]), provide high wear resistance, stability under high-service temperatures, corrosion resistance, and low thermal conductivity; recently, interstitial nitrides like vanadium nitride (VN) and hafnium nitride (HfN) are being studied because of their interesting properties such as high hardness, elastic modulus, low friction coefficient, as well as wear and corrosion resistance, [6–9]. In recent years multilayer systems based on nitride coatings such as TiN/ZrN [10], TiN/VN, Hf/HfN and W/WN [11,12] have been deposited as multilayer systems. These systems have shown good results specifically related to improved mechanical properties and oxidation resistance, as compared to the single layer, e.g., CrAlN and TiAlN coatings [13,14]. Enhancement of these properties is attributed to different mechanisms of layer formation with nanometric thickness such as the Hall–Petch effect and interface numbers acting as obstacles for the inward and outward diffusion of atomic species between layers for oxidation resistance or dissipation of crack energy in the case of toughness [15]. However, there are still very few studies in literature reporting on the electrochemical responses in nanostructured systems based on isostructural assembly of nitride coatings generated by metal transition. Considering this for the current research, Si (100) and AISI 4140 steel substrates were coated with a set of HfN/VN multilayers with a bilayer period (Λ) between 1200 and 15 nm (n = 1–80), for 1.2-μm total thickness. Therefore, the principal objective of this work is to evaluate the mechanical and corrosion resistance evolution of nanostructured multilayered HfN/VN coatings with the influence of HfN/VN deposited onto silicon (100) and industrial AISI 4140 steel substrates with different bilayer periods, Λ, and bilayer numbers, n, on their physical nature compared with uncoated industrial steel. The results are shown in this paper for possible surface applications in processes with aggressive environments such as in metals used in the mechanical industry.

2. Experimental details

Hafnium nitride/vanadium nitride multilayered system was grown on Si (100) and AISI 4140 steel substrates by using a multi-target magnetron sputtering system, with an r.f. source (13.56 MHz). The plasma cleaning procedure was used for all substrates under argon atmospheres. Two metallic targets hafnium (Hf) and vanadium (V) with

* Corresponding author. Tel.: +57 2 3384610; fax: +57 2 3393237.
E-mail address: jcaicedoangulo1@gmail.com (J.C. Caicedo).

0257-8972/$ – see front matter © 2013 Elsevier B.V. All rights reserved.
http://dx.doi.org/10.1016/j.surfcoat.2013.02.002

99.9% purity were used as source materials. The deposition parameters to obtain VN and HfN films had a sputtering power of 400 W for V and 350 W for the Hf target; an unbalanced r.f. bias voltage was applied which generated a negative signal fixed at −30 V and a substrate temperature of 250 ºC under 60 rpm circular rotation substrate to facilitate the formation of the stoichiometric films. The sputtering gas was a mixture of Ar 80% and N_2 20% with a total working pressure of 0.12 Pa. The gases used were of ultra-high purity (99.999%). Film thickness was measured at approximately 1.2±0.1 μm, determined by means of a (Dektak 3030) Profilometer. The crystal structure of the films was determined by using a Panalytical X'Pert PRO X-ray diffractometer with Cu-Kα radiation (λ = 1.5405 Å). The bilayer period and multilayer assembly modulation was observed via scanning electron microscopy (SEM, 6490 LV JEOL). Microstructural analysis of films was mainly performed by TEM, using a Philips CM30 microscope operating at 300 kV.

In this work the HfN/VN multilayer on silicon (100) substrate was deposited at the same time that the HfN/VN multilayer is deposited on the steel substrate, but the HfN/VN multilayer on the silicon (100) substrate was used because this substrate facilitates the experimental characterization via XRD, XPS, SEM and TEM techniques.

The electrochemical study was performed by using a Gamry unit; model PCI 4, utilized for DC and AC measurements. Electrochemical Impedance Spectroscopy (EIS) and Tafel polarization curves were obtained at room temperature (25 C) under static conditions (without aeration), using a cell with a working electrode of 1-cm^2 exposed area, Ag/AgCl (3.33 M KCl) reference electrode, and a platinum wire counter-electrode under a 3.5 wt.% NaCl solution with distilled water at pH 6.2. For Nyquist plots, frequency sweeps were conducted in the range of 100 kHz to 0.001 Hz using sinusoidal signal amplitude of 10 mV applied to the working electrode (sample) and the reference electrode. Diagrams for Tafel polarization curves were obtained at a sweep speed of 0.125 mV/s in a voltage range of −1000 to 1000 $mV_{Ag/AgCl}$; this voltage range was defined with respect to the open circuit potential (OCP). Prior to beginning the polarization curve procedures, the samples were submerged in the 3.5 wt.% NaCl aqueous solution for 30 min to establish the free corrosion potential values (E_{corr}) where polarization curve measurements were initiated. In this work, the surface corrosion process was carried out, analyzing surface morphology by using a 50×-objective optical Olympus PME-3 microscope and a Scanning Electron Microscope (SEM) (Phenom FEI) equipped with a light optical magnification range: 525–24× and a height sensitivity back-scattered electron detector (multi-mode).

3. Results and discussion

3.1. X-ray analyses of HfN/VN system

XRD diffraction of hafnium nitride/vanadium nitride deposited onto a Si (100) substrate with Λ between 1200 nm and 15 nm and n between 1 and 80 is shown in Fig. 1a. VN and HfN layers within the multilayered systems were polycrystalline, exhibiting diffraction peaks with a preferential orientation (111) corresponding to the HfN phase located at 34.01°; other peaks were observed at 68.06° and 71.67°, corresponding to the (311) and (222) planes, respectively. These were attributed to the HfN structure. The diffraction peaks at 44.23° and 38.09°, corresponded to the (200) and (111) VN planes, respectively. Comparatively, in Fig. 1b the shift of diffraction patterns towards high angles is in relation to compressive residual stress characteristics for those multilayered systems (Table 1). These preferential orientations are in agreement with JCPDS 00-035-0768 (VN) and JCPDS 00-033-0592 (HfN) from ICDD cards. Moreover, it was observed that the HfN (111) peak position suffers slight deviation from the bulk value, indicating a possible stress relief of HfN/VN multilayers with a thinner bilayer period (Λ = 15 nm; n = 80).

3.2. XPS analysis for HfN and VN single layers

The XPS survey spectrums for HfN and VN single layers that make up the HfN/VN multilayer coatings are shown in Fig. 2. For HfN material in Fig. 2a the peaks at 523.2 eV, 397.6 eV, 224.8 eV and 18.4 eV correspond to O1s, N1s, Hf4d5, and Hf4f binding energies, respectively. The change of binding energy of the HfN verifies the formation of binary Hf(N) compounds, therefore, calculation of the peak area gives an atomic ratio of Hf:N = 1.1:0.9, which is similar to the stoichiometry of $Hf_{1.1}N_{0.9}$ [16]. Comparatively, Fig. 2b shows the peaks of VN material at 630.4 eV, 532.0 eV, 516.8 eV, and 397.6 eV corresponding to V2s, O1s, V2p3/2, and N1s binding energies, respectively. The change of binding energy of VN verifies the formation of binary V(N) compounds, therefore, calculation of the peak area gives an atomic ratio of V:N = 1.1:0.9, which is similar to the stoichiometry of $V_{1.2}N_{0.8}$ material [17].

According to the XPS literature on Hf-N and V-N materials [16,17] when peaks are fitted from experimental results it is necessary to first adjust the N energy band because it is the element that provides greater reliability for XPS, then take this initial adjustment as the base and the other peaks related to the remaining elements are

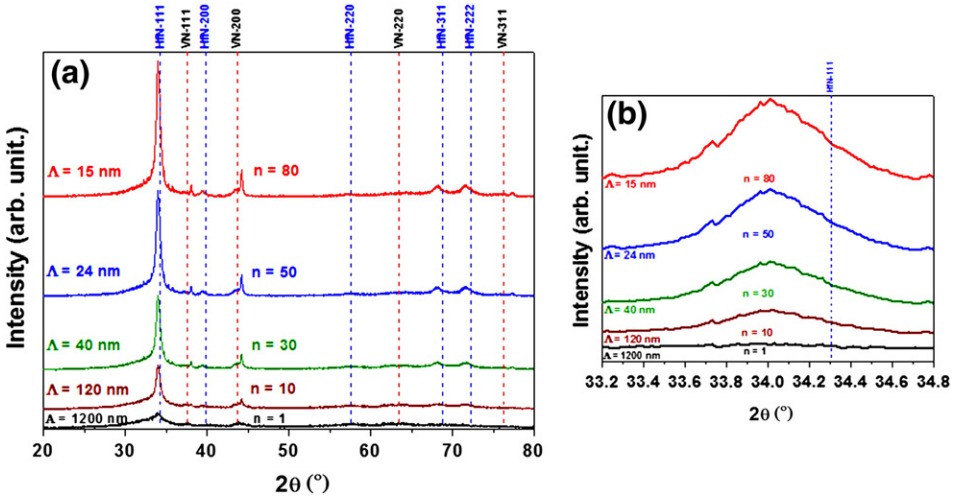

Fig. 1. The XRD patterns of the HfN/VN multilayered coatings deposited on Si (100) substrates with Λ between 1200 nm and 15 nm and n between 1 and 80: (a) dashed lines indicate the position of the peaks obtained from JCPDS 00-035-0768 (VN) and JCPDS 00-033-0592 (HfN) files from ICDD cards and (b) maximum peak with shift toward high angles in relation to increasing bilayer numbers (n).

Table 1
2θ peak and intensity peak for different bilayer periods for $[HfN/VN]_n$ multilayered.

	n = 1	n = 10	n = 30	n = 50	n = 80
2θ peak (°)	33.91	33.96	33.98	33.99	34.01
Intensity peak (%)	36.7	44.1	55.1	68.5	87.7

therefore adjusted. The latter is necessary due to the characteristics that are present in this kind of insulating material (coating) with respect to the incident signal, in this way avoiding the uncertainties caused by the charging and shifts of the Fermi energy. Thus, the concentration measurements and identification of the specific bonding configurations for HfN and VN layers are more reliable. Therefore, the core electronic spectra that carry the information of the chemical composition and bonding characters of the HfN and VN films increase the reliability of the results.

3.3. Scanning electron microscopy analysis for [HfN/VN]n multilayered

A first glimpse on $[HfN/VN]_n$ multilayer modulation and microstructure was accomplished by SEM micrographs. Fig. 3 presents the cross-sectional image of a $[HfN/VN]_n$ coating with n = 10 and Λ = 120 nm. The darkest contrast of VN layers with respect to HfN layers allowed for a clear determination of the layer structure. These $[HfN/VN]_{10}$ coatings (Fig. 3a) presented a buffer layer of Hf with a thickness of approximately 90 nm, the HfN/VN multilayer with total thickness around 1.2 μm with well-defined and uniform periodicity. The high SEM resolution for multilayer coatings is shown in Fig. 3b for $[HfN/VN]_{30}$ deposited with Λ = 40 nm, exhibiting a clear multilayer contrast corresponding to a different density with a perfect modulation of the multilayer system. All multilayer stacks were resolved by SEM and confirmed quite precisely the previously designed values of the bilayer thickness, as well as the total thicknesses. The only slight deviation observed by SEM imaging was on relative thicknesses.

3.4. Transmission electron microscopy analysis

The atomic microstructures were accomplished by HRTEM images. Fig. 4 shows the TEM cross-sectional image of HfN/VN coating. The interplanar distance in both materials (HfN–VN) was confirmed using transmission electron microscopy. TEM images show that the interplanar distance of HfN layer (d = 0.2612 nm) is marginally lower than the VN layer (d = 0.2060 nm); they also confirmed that the interplanar distance in VN layer is 0.0552 nm narrower than the HfN layer. It reveals a compact crystalline structure with wide columnar grains extended along the entire layer stack. The region shown in Fig. 4 enabled us to study the structure of a single crystallite which can be identified as a small dark zone propagating through the film.

3.5. Electrochemical impedance spectroscopy (EIS) and Tafel polarization curves

Fig. 5 displays the Nyquist diagram, imaginary part of the impedance versus its real part, for the $[HfN/VN]_n$ multilayers grown at different bilayer periods and bilayer numbers: n = 1 (open circle symbol), n = 10 (filled square), n = 30 (filled down triangle), n = 50 (filled stars), n = 80 (filled triangle) and for the uncoated AISI 4140 steel substrate (filled circle). A strong dependency of the Nyquist diagrams related to bilayer number (n) from $Z_{real}(Z_{imag} = 0)$ to $Z_{real}(Z_{imag}max)$ with the intercept of the curve with Z_{real} axis was observed, therefore, to fit experimental data, the system provides a equivalent circuit [18], simulating the substrate-coating and coating-electrolyte interfaces as a double-layer capacitance in parallel with the coating resistance and electrolyte resistance due to the ion reaction transfer [19,20] from the electrolyte to the metallic substrate.

In all corresponding Bode diagrams of the multilayer capacitive, the behavior was observed at high frequencies. This phenomenon is associated with turning a dispersion process in frequency because the electrode surface is not homogeneous. Additionally, there is a diffusion process that aims to define a second inflection at low frequencies. Table 2 shows the values of the parameters used in the simulation. Also, included were the parameters used in the simulation.

The values of these capacitive parameters were obtained through a non-complex linear least squares (CNLS) program. Fig. 6 shows the equivalent circuit corresponding to the Bode plots for the coatings, which show a capacitance called "constant phase element dual phase" (CPE), which is independent of faradic reaction, which contributes a pseudocapacitance (CPE2 + CPE1) to the total system impedance.

Moreover, in this electrochemical cell there is also an electrical resistance associated with the electrolyte resistance (Rs) that will be equally evident in the total system impedance. The values of α (Table 2), correspond to the coefficient exponential phase shift angle (π/2) α values; for the coatings and the substrate for CPE to high frequency values are in the range of 0.73 KHz and 0.86 KHz indicating that the surface roughness produces a load distribution for the low frequency CPE which

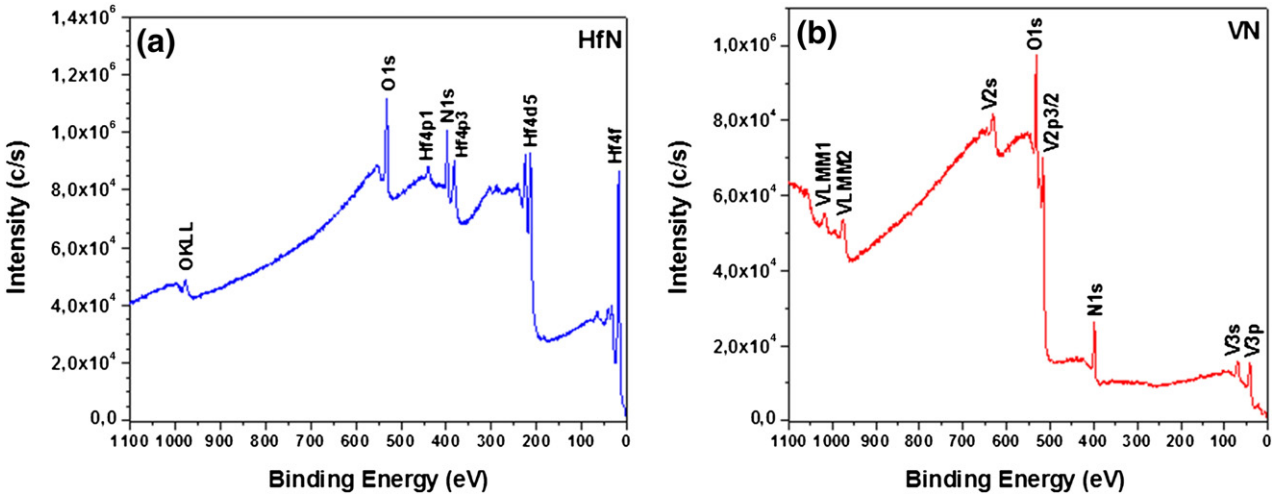

Fig. 2. XPS survey spectrums (a) HfN coatings and (b) VN coatings deposited on Si with an r.f. negative bias voltage of −30 V.

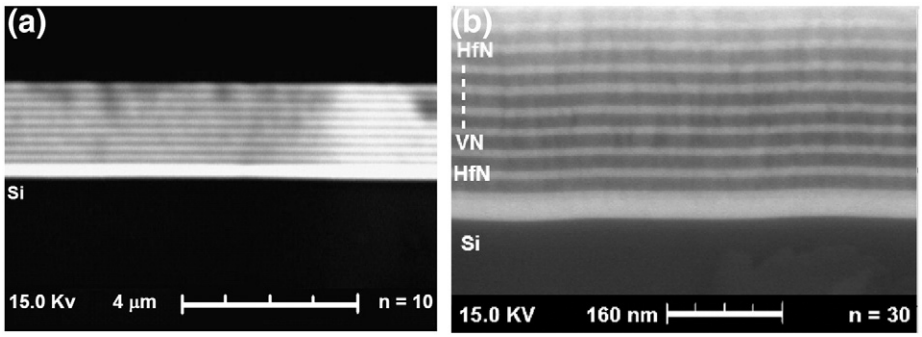

Fig. 3. SEM micrograph of HfN/VN multilayer system, (a) coating deposited with n = 10, Λ = 120 nm, (b) coating deposited with n = 30, Λ = 40nm.

shows an α, of 0.68 to 0.72 and n = 1 to n = 10, respectively. Considering this it is possible to observe a migration or diffusion species, for n = 30, n = 50 and n = 80 associate to α values of 0.87, 0.81 and 0.92, respectively, thereby generating a distribution of the charge carrier density, ie. a double layer with a complex structure.

From the Nyquist diagrams and the equivalent circuit (Fig. 7) values were extracted for polarization resistance (RP). The results in Tables 2 and 3 indicate that polarization resistance increases when bilayer numbers increase for $[HfN/VN]_n$ multilayered coatings. The equivalent circuit contains two distributed constant-phase elements (CPE_1 and CPE_2) to consider the two relaxation time constants. The CPE_1–R_1 coupling, predominating at high frequencies, may have originated by the passive film and/or the dielectric properties of the multilayers; while the CPE_2–R_2 coupling, controlled at low frequencies, characterizes the corrosion process of the steel/multilayer pore solution interface. RE is the electrolyte resistance. The distributions of CPEs are widely used in data fitting because they allow for analysis of the depressed semicircles. The depressed semicircle is generally due to a dispersion in the time constant caused by irregularities on the steel surface, surface roughness, fractal surface, and in general certain processes associated with an irregular distribution of the applied potential (10 mV) to obtain the EIS data.

Table 2 shows the theoretical calculations of the total impedance values, which are equivalent to the simulated data with the equivalent circuit (Fig. 7). The substrate has only one inflection and this effect is due to the oxide layer that is formed from the contact of the steel with the aggressive solution to which it is subjected. The total impedance data, best known as the sum of the resistances Rp1 + Rp2, increase with the increase of bilayer numbers (Table 3). It is observed in this paper that the values of (Rp1 + Rp2) are much higher than those found in the substrate because the electrolyte is very aggressive and generates a higher reaction rate on the uncoated steel.

The admittance representation of a CPE (Y_{CPE}) shows a dependent fractional-power on the angular frequency (ω): $Y_{CPE} = Y_P(j\omega)^{\alpha}$, where Y_P is a real adjustable constant used in the non-linear least squares (NLLS) fitting, and $-1 < \alpha < 1$ is defined as a CPE power [21]. So, when $\alpha = 0$ CPE is a resistor, when $\alpha = 1$ it is an ideal capacitor, and when $\alpha = -1$ it is an inductor. Finally, if $\alpha = 0.5$ CPE is the Warburg admittance.

Tafel polarization curves and the corrosion potential as a function of the corrosion current density for $[HfN/VN]_n$ multilayered coatings at different bilayer periods (Λ) are shown in Fig. 8. Tafel polarization curves have been used to calculate surface corrosion rate.

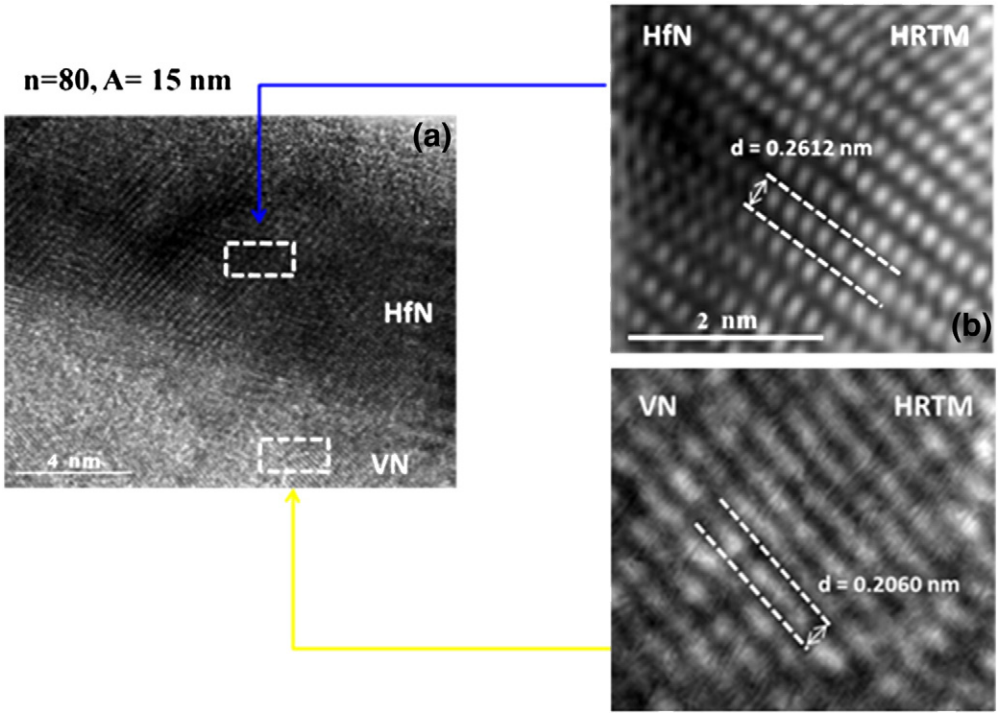

Fig. 4. (a) TEM image of HfN/VN multilayer coatings with n = 80, Λ = 15 nm, atomic microstructures of HfN (b) and VN (c) layers.

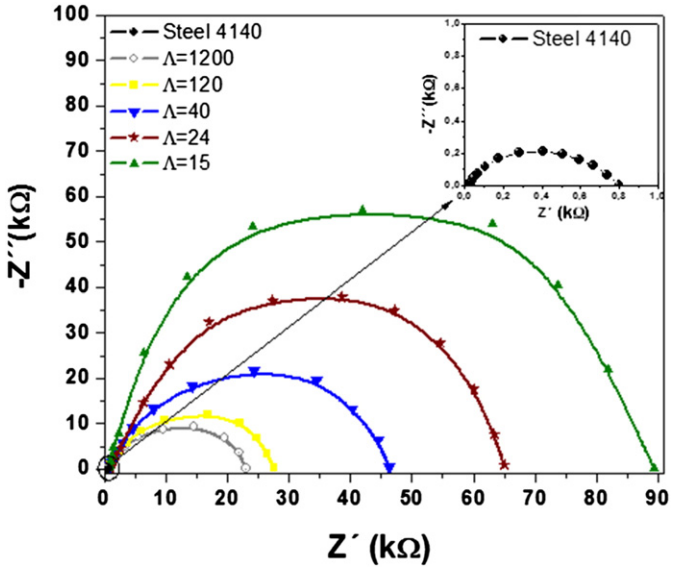

Fig. 5. Impedance diagrams of $[HfN/VN]_n$ multilayers grown at different bilayer periods (Λ) on AISI 4140 steel.

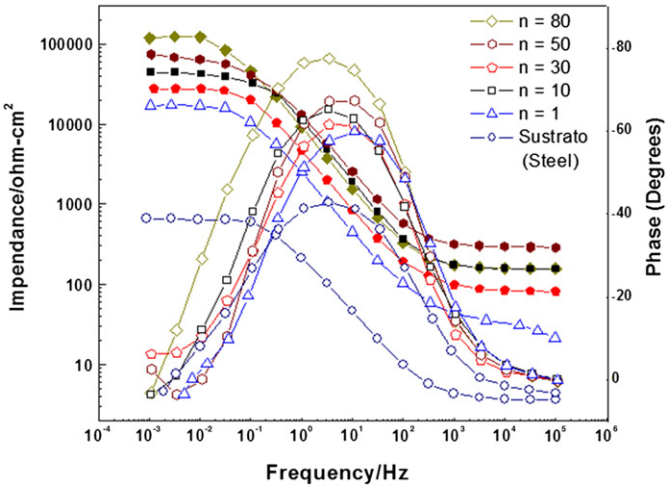

Fig. 6. Bode diagrams for HfN/VN coating systems as a function of bilayer numbers (n).

Tafel polarization curves are strongly dependent on the Λ and/or n, indicating the influence of interfaces present within multilayers. These curves allow finding anodic and cathodic slope values in each case which are necessary to calculate a correct value of the corrosion rate for all systems.

The corrosion potentials of the coated steel are more electropositive when the bilayer number is increased with respect to the uncoated steel confirming the protective effects of the coatings. This behavior is a characteristic of multilayered structures [22–24]; as a consequence of increasing bilayer numbers (n), the density and the interface numbers are also increased for a thoroughly uniform thickness of the multilayered system; thus, the number of pores is reduced. This leads to the observation that the energy required for Cl^- ion movement across the coating/substrate interface with freedom is higher; therefore, the ions arriving to the substrate are less due to the change of direction experienced by Cl^- ions than when these find a new interface [25]. Moreover, the chemical composition in the interface for both nitride layers observed by XPS results (Fig. 2) produced a different interfacial molecular potential associated with (HfN–VN) chemical interaction and changes in the interplanar spacing (d). When new interface between HfN and VN layers are generated, as observed in TEM results (Fig. 4), lower current corrosion density is observed, it is probably due to the number of interfaces increased. More micro-pores and microcracks are blocked; therefore, to cross the coating high transition energy is required for the corrosive Cl^- ions [26]. Polarization resistance values were found with the Nyquist diagrams used to calculate corrosion rates from the polarization curves, both values are shown in Table 2. These values clearly show that the polarization resistance of AISI 4140 was improved when the steel was coated with $[HfN/VN]_{80}$ (Λ = 15 nm); this observation agrees with the literature on enhanced properties of steel substrates by using multilayered coatings [24–26].

The scientific literature for novel multilayer system HFN/VN had not reported corrosion studies; moreover, in this research atomic interfaces in the HFN and VN were observed by TEM, which was related to the corrosion mechanism and evolution evidenced in corrosion resistance, eg, the [HfN/VN]n presents a corrosion resistance higher than 2 times the [TiN/TiAlN]n system with similar multilayer number [24].

Fig. 9 shows the electrochemical properties of $[HfN/VN]_n$ multilayers. Fig. 9a shows a clear trend of polarization resistance (R_P) as a function of bilayer number and bilayer period. Fig. 8b shows the corrosion rate (V_c) as a function of the increased bilayer number (n) or the increased interface number due to the reduction of bilayer period (Λ) in $[HfN/VN]_n$ multilayers. Additionally, Fig. 9a shows the systematic dependence of the bilayer numbers compared to R_P, given that the uncoated AISI 4140 steel substrate presents the lowest corrosion resistance compared to the steel coated with one bilayer (Λ = 1200 nm). When analyzed, the multilayer coatings deposited with 80 bilayers (Λ = 15 nm) presented the highest R_P due to higher interface numbers (n). Moreover, the corrosion rate (V_c) showed a dramatic increase for the uncoated steel substrate, which differs for steel coated with one bilayer (Λ = 1200 nm), where it is possible to find a reduction in the lower corrosion rate. Also, coatings deposited with 80 bilayers (Λ = 15 nm) exhibit less (V_c), with respect to all

Table 2
Parameters used to calculate the corrosion rate for HfN/VN coating system.

	R_s Ω cm²	CPE_1 μF cm^{-2} $s^{-(1-\alpha 1)}$	α_1	Rp_1 Ω cm²	CPE_2 μF cm^{-2} $s^{-(1-\alpha 2)}$	α_2	Rp_2 10^3Ω cm²
n = 80	154.2	7.80	0.82	1530.40	69.34	0.92	118.16
	(0.5%)	(4%)	(0.2%)	(2%)	(2%)	(0.4%)	(6%)
n = 50	287.4	6.90	0.80	2510.30	48.23	0.81	73.21
	(0.3%)	(1%)	(0.3%)	(3%)	(4%)	(0.3%)	(3%)
n = 30	162.3	6.40	0.81	795.60	39.45	0.87	43.24
	(0.4%)	(3%)	(0.3%)	(2%)	(4%)	(0.4%)	(5%)
n = 10	154.7	5.68	0.73	373.40	36.76	0.72	27.31
	(0.2%)	(3%)	(0.4%)	(3%)	(4%)	(0.5%)	(3%)
n = 1	81.2	3.49	0.76	102.20	31.23	0.68	16.74
	(0.2%)	(2%)	(0.5%)	(2%)	(4%)	(0.6%)	(4%)
Steel 4140	3.6	1.98	0.86	650.10	–	–	–
	(0.8%)	(1.5%)	(0.9%)	(3%)			

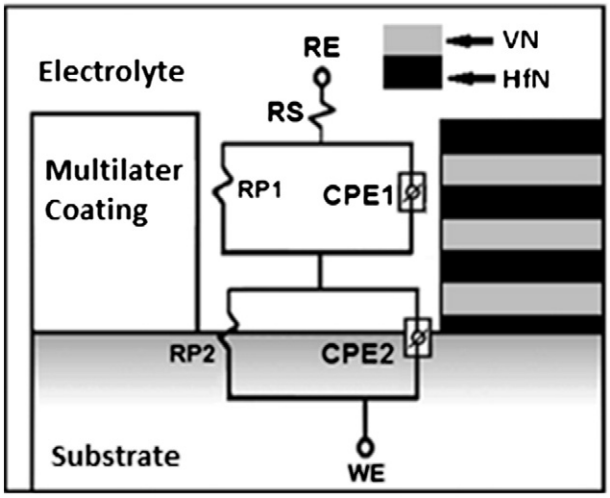

Fig. 7. Equivalent circuits used for simulation of the experimental data in electrochemical characterization of $[HfN/VN]_n$ multilayers; reference electrode (RE), electrolyte resistance (RS), polarization resistance (RP) (multilayered films), constant phase elements (CPE), and working electrode (WE).

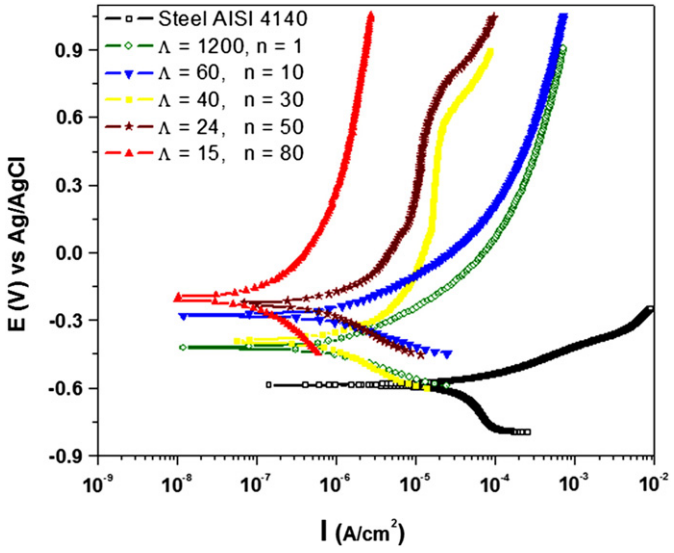

Fig. 8. Tafel curves of $[HfN/VN]_n$ multilayers grown at different bilayer periods (Λ) on AISI4140 steel.

multilayered systems shown in this work, as presented in the previous discussion.

Moreover, in research Figs. 5 and 7 show the impedance diagrams and the Tafel plots of [HfN/VN]n multilayered grown at different bilayer periods (Λ) on AISI 4140 steel which are presented respectively, because the steel studied in this paper is used industrially in harsh environments where steel can be attacked by the corrosive effect, which does not happen with a ceramic silicon substrate. Furthermore, the aim of the paper is not to assess the influence of the substrate in physical and electrochemical properties.

This paper found that the lower residual stress which was observed via XRD (Fig. 1) results is in agreement with the lower corrosion rate determined by EIS results (Fig. 5) when the bilayer number (n) was increased, thus showing better electrochemical properties, because the residual stress can generate internal microcracks and micro-pores [5].

3.6. Surface corrosion analysis by optical microscopy and SEM

With the goal of observing the corrosive damage suffered by the coated samples with HfN/VN multilayered, a microscopic analysis of the surfaces on the samples was conducted immediately after finishing the electrochemical measurements via optical and scanning electron microscopy. Fig. 10a–e, shows optical micrographs on the surface multilayered coatings after following identical electrochemical processes. Images were taken under identical conditions of amplification and illumination. The images clearly display the degradation of the surface due to the NaCl solution chemical attack at the HfN/VN multilayered coatings grown with a r.f. negative bias voltage of −30 V, the biggest chemical attack (darker zone) was found when coating with bilayer number (n = 1) (Fig. 10a). Evidently, the degradation levels depended on the type of multilayered coatings (Λ), indicating that the multilayered coatings grown with (n = 80, Λ = 15 nm) are the most appropriate coatings for reducing corrosion processes in steel. The interfaces layered within multilayered coatings have an important contribution to reduction of the chemical attack, possibly due to its change of direction experienced by Cl^- ions allowing an electrochemical potential that promotes resistance to corrosion because the reduction of porosity in multilayered is even more significant in all electrochemical systems with lower corrosion rates than the coatings deposited with lowest bilayered number (n) or lowest interface number [21].

The scanning electron microscopy (SEM) images of the surface degradation processes produced by NaCl solution attack on $[HfN/VN]_n$ multilayered are shown in Fig. 11a–e.

The corrosion process caused catastrophic effects on the steel substrate surface and surface multilayered coatings with lowest interface number (n = 1); thus generating a partial delamination of coating, which allowed the evolution of corrosion mechanisms between aggressive environments and the substrate surfaces (Fig. 11a), together with (Fig. 11b). Fig. 11c shows a reduced surface attack on steel substrates coated with n = 30 (Λ = 40 nm) compared to Fig. 11a–b, but some areas have also suffered delamination. In contrast, in Fig. 11c the corroded areas in the sample surface coated with n = 50 (Λ = 24 nm) are drastically reduced, as well observed was a pitting type damage due to some defects at the coatings (e.g., pores, cracks, etc.), generated in the deposition process, specifically, from the use of bias voltage as shown in [25]. The sample that provides the best resistance to electrochemical attacks is the multilayered coating grown with the highest bilayer number (n), highest interface number and lowest bilayer period (Λ) (n = 80, Λ = 15 nm), since these multilayered coatings exhibit very low susceptibility to pitting corrosion (Fig. 11e).

A sample providing the best resistance to electrochemical attack is the coating grown with the highest bilayer number and the lowest bilayer period, n = 80, Λ = 15 nm (Fig. 11e). The coating grown with the lowest bilayer number (n = 1, Λ = 1200 nm), Fig. 11a, shows that the corrosion process causes catastrophic effects on the surface coatings generating bite damage and breaking the coating continuity (dark zones).

Additionally, seeking to confirm the observed SEM images, a porosity factor associated to the different coatings was calculated in

Table 3
Polarization resistance, corrosion rate, and porosity for steel and $[HfN/VN]_n$ multilayered.

	Steel 4140	n = 1	n = 10	n = 30	n = 50	n = 80
RP (kΩ cm^2)	0.650	23.92	27.68	46.36	72.42	112.19
Corrosion rate (mmy)	0.014	$0.758*10^{-3}$	$0.586*10^{-3}$	$0.477*10^{-3}$	$0.261*10^{-3}$	$0.094*10^{-3}$

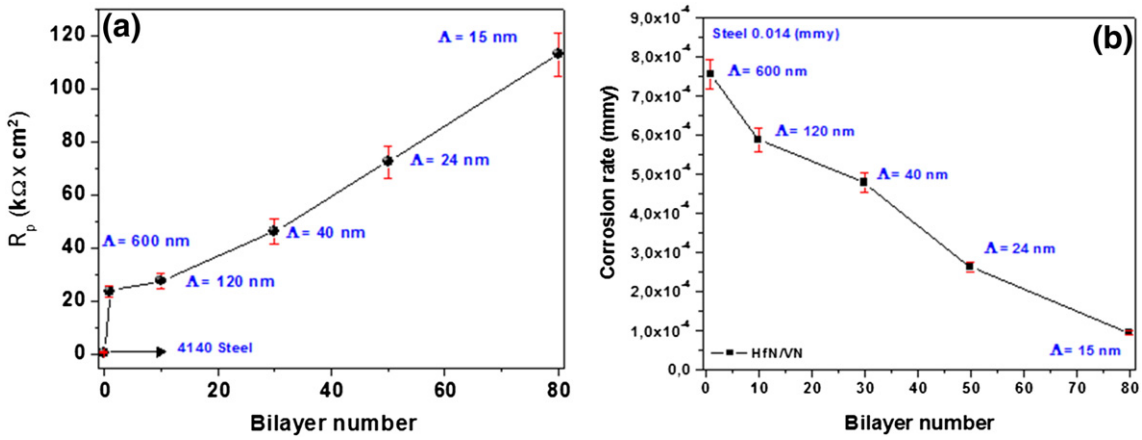

Fig. 9. Electrochemical properties for $[HfN/VN]_n$ multilayers: (a) polarization resistance as a function of bilayer number or bilayer period, (b) corrosion rate as a function of bilayer number or bilayer period.

agreement with Tato et al. [27]; porosity factor corresponds to the ratio between polarization resistance of the uncoated substrate and the coated substrate, as shown in Eq. (1):

$$P = \frac{R_{p,u}}{R_{p,r-u}} \tag{1}$$

where P is the total coating porosity, $R_{p,u}$ is the polarization resistance of the uncoated substrate, and $R_{p,r-u}$ is the measured polarization resistance of the coating–substrate system. The polarization resistance values used in Eq. (1) correspond to the values extracted from the Nyquist diagrams; specifically, they were extracted from the equivalent circuits determined in each case. From different studies reported in the literature [28,29] coatings deposited by PVD techniques are stressed and have defects (e.g., pores and cracks). Considering this, it is assumed that the contact between the electrolyte and the steel substrate takes place only through the pores in the coating, the latter to make the analysis simple. Therefore, with Eq. (1), only the effect of the coating on the increased polarization resistance on the steel was evaluated. If the value of the porosity factor is close to zero (0%), it indicates that the coating acts as an inert barrier against the corrosive solution. Conversely, if the porosity factor is close to unity (100%) it indicates that the coating does not act as a barrier for the diffusion of Cl^- corrosive ions and this behavior is attributed to the coating porosity.

Fig. 12 presents the porosity factor (coating porosity) values obtained by replacing the electrochemical values on Eq. (1) for all multilayered coatings. The analysis of porosity factor values applied in all coatings suggests that the porosity factor decreased with an increased bilayer number (n) or with an increased interface number. Moreover, these results are in agreement with the reduction of corrosion rate observed in $[HfN/VN]_n$ multilayers and the SEM images in Fig. 12. Finally, according to our findings, as the bilayer number (n) or interface number increases, the density is also increased for a thoroughly uniform thickness of the multilayered system. This leads to the observation that the energy required for Cl^- ion movement across the coating/substrate interface with freedom is higher; therefore, the ions arriving to the substrate are less due to the change of direction experienced by Cl^- ions when these find a new interface.

Taking into account that bilayer period (Λ) represents the sum of the individual thicknesses ($\Lambda = t_{HfN} + t_{VN}$) of the single layers comprising the multilayer system, it is expected that the multilayer

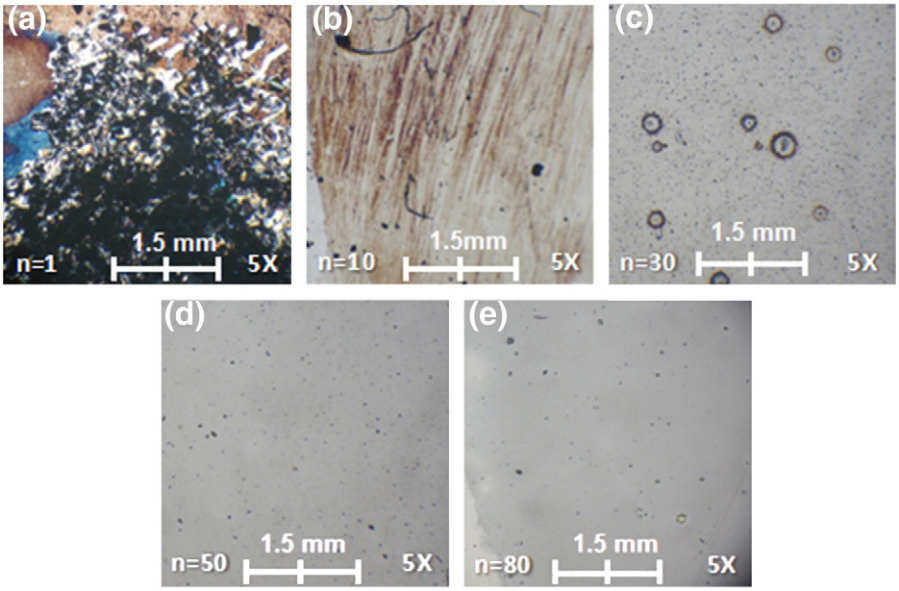

Fig. 10. Optical microscopy images showing degradation of the surface in $[HfN/VN]_n$ multilayered coatings after identical electrochemical processes: (a) n = 1 (Λ = 1200 nm); (b) n = 10, (Λ = 120 nm); (c) n = 30, (Λ = 40 nm); (d) n = 50, (Λ = 24 nm); (e) n = 80, (Λ = 15 nm).

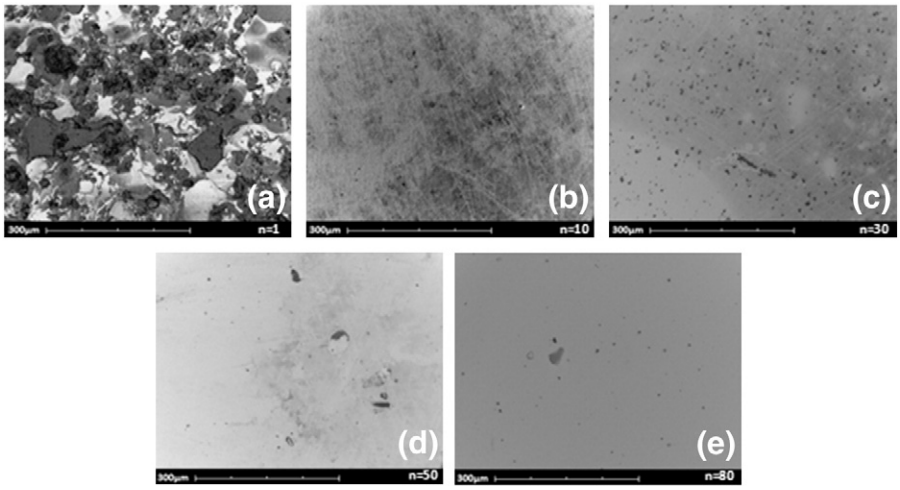

Fig. 11. SEM images showing degradation of the surface in $[HfN/VN]_n$ multilayered coatings after identical electrochemical processes; (a) n = 1, (Λ = 1200 nm); (b) n = 10, (Λ = 120 nm); (c) n = 30, (Λ = 40 nm); (d) n = 50, (Λ = 24 nm); and (e) n = 80, (Λ = 15 nm).

system with the lower Λ exhibits the best corrosion resistance, as shown in this paper.

3.7. The protective efficiency film

The protective efficiency of the $[HfN/VN]_n$ multilayers is found by observing the surface nature and taking into account the electrochemical nature of the coating, therefore, the protective efficiency factor associated with the different films is in agreement with Caicedo and coworkers [30]; in this sense, the protective efficiency factor corresponds to the ratio of the difference between corrosion intensity of the uncoated steel substrate and the corrosion intensity for the coated steel substrate divided by corrosion intensity of the uncoated steel substrate, which is shown in the following equation:

$$Pf(\%) = \left(\frac{Icorr_S - Icorr_f}{Icorr_S}\right) \times 100 \quad (2)$$

where *Pf* is the protective efficiency factor, $Icorr_s$ is the corrosion intensity of the uncoated steel substrate, and $Icorr_f$ is the corrosion intensity of the coated substrate. The protective efficiency factor values were obtained in Fig. 13, replacing the electrochemical values on Eq. (2) for all multilayers. The analysis of protective efficiency factor values applied in these multilayers, suggests that the protective efficiency factor is determined for $[HfN/VN]_n$ multilayer systems, evidencing a better behavior when the bilayer number is increased, and the best protective nature corresponding to the multilayered coatings grown with n = 80, Λ = 15 nm, moreover, these results are in agreement with polarization resistance (Fig. 9a), corrosion rate (Fig. 9b), SEM micrographs (Fig. 11), and the porosity factor values presented in Table 3.

In this current research it was analyzed that the porosity factor (100% means no coating and 0% means full coverage), therefore, these effects are in relation to physical properties which are evidenced with residual stress observed by XRD results (Fig. 1) and observed by SEM images (Fig. 10); moreover, the porosity factor can be co-related to the electrochemical nature of the coating associated to free ion migration by pores facility. So, on the other hand, the protective efficiency effects are in relation to the chemical properties which are evidenced with the chemical interaction between nitride coatings and corrosive electrolytes. Moreover, the protective efficiency, opposite to the porosity factor, is related to the electrochemical nature of the coating and not to the presence of porosity (defects) as discussed in Section 3.6.

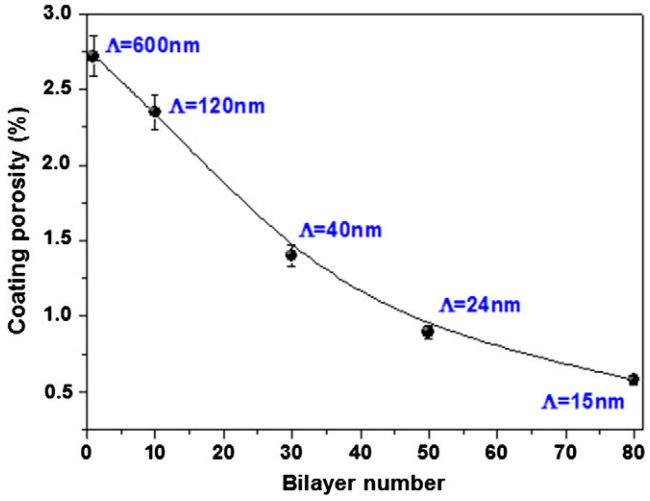

Fig. 12. Coating porosity as function of increased bilayer number (n) or decreased bilayer period (Λ).

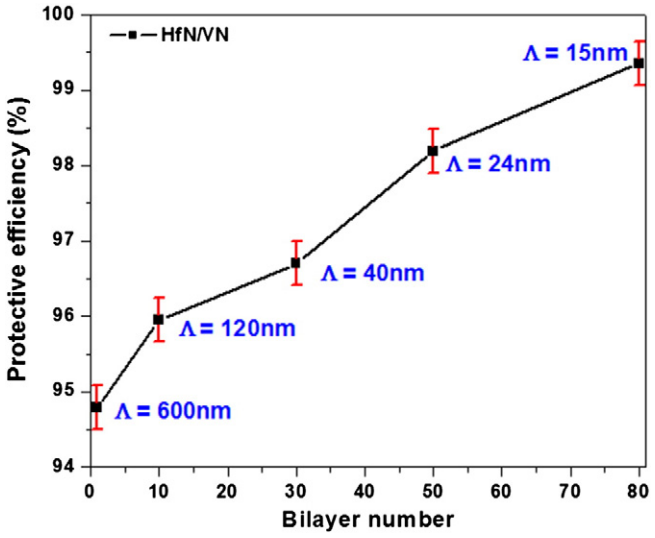

Fig. 13. Protective efficiency for $[HfN/VN]_n$ multilayered as function of bilayer number (n).

4. Conclusions

Hafnium nitride/vanadium nitride multilayered systems were successfully deposited onto AISI 4140 steel substrates by r.f. multi-target magnetron sputtering process, with bilayer periods ranging from 1200 to 15 nm. The SEM and TEM micrographs showed multilayer evidence with well-defined and uniform periodicity. Multilayered coatings enhanced corrosion properties, increased the corrosion resistance and reduced the corrosion rate as compared to the uncoated industrial AISI 4140 steel.

The multilayered coatings showed enhanced corrosion resistance caused by the effect of the interfaces that generated a protective layer over the steel substrate, creating a higher resistance to corrosion compared to uncoated steel. The $[HfN/VN]_{80}$ multilayered coatings exhibited lower porosity and bilayer period ($\Lambda = 15$ nm) resulting in effective barriers for the diffusion of reactive species. Therefore, the optimal conduction was found when the multilayer coating showed the lower bilayer period.

Acknowledgements

This research was supported by "El patrimonio Autónomo Fondo Nacional de Financiamiento para la Ciencia, la Tecnología y la Innovación Francisco José de Caldas" under contract RC-No. 275-2011 and the program "Jóvenes Investigadores e Innovadores Virginia Gutiérrez de Pineda" No. 525-2011. Moreover, the authors acknowledge the Serveis Científico-Técnics of the Universitat de Barcelona.

References

[1] B. Podgornik, J. Vizintin, Vacuum 68 (1) (2002) 39.
[2] P. Hovsepian, Q. Luo, G. Robinson, M. Pittman, M. Howarth, D. Doerwald, R. Tietema, W.M. Sim, A. Deeming, T. Zeus, Surf. Coat. Technol. l.201 (2006) 265.
[3] J. Korean Phys. Soc. 56 (3) (March 2010) 905.
[4] A. Glaser, S. Surnev, F.P. Netzer, N. Fateh, G.A. Fontalvo, C. Mitterer, Surf. Sci. 601 (2007) 1153.
[5] J.C. Caicedo, C. Amaya, L. Yate, M.E. Gómez, G. Zambrano, J. Alvarado-Rivera, J. Muñoz-Saldaña, Appl. Surf. Sci. 256 (20) (Aug. 2010) 5898.
[6] M. Staia, D. Bhat, E. Puchicabrera, J. Bost, Wear 261 (5–6) (Sep. 2006) 540.
[7] H.O. Gekonde, S.V. Subramanian, Surf. Coat. Technol. 149 (2–3) (Jan. 2002) 151.
[8] G. Gassner, P.H. Mayrhofer, K. Kutschej, C. Mitterer, M. Kathrein, "A new low friction concept for high temperatures: lubricious oxide formation on sputtered VN coatings", Tribol. Lett. vol. 17, no. 4, (2004) 751–756.
[9] N. Fateh, G.A. Fontalvo, G. Gassner, C. Mitterer, Wear 262 (9–10) (Apr. 2007) 1152.
[10] J.C. Caicedo, C. Amaya, L. Yate, O. Nos, M.E. Gómez, P. Prieto, Mater. Sci. Eng. B 171 (2010) 56.
[11] U. Helmersson, S. Todorova, S.A. Barnett, J. Sundgren, L.C. Markert, J.E. Greene, J. Appl. Phys. 62 (1987) 481.
[12] K.K. Shih, Appl. Phys. Lett. 61 (1992) 654.
[13] L.A. Dobrzañski, K. Lukaszkowicz, Arch. Mater. Sci. Eng. 28 (2007) 549.
[14] C. Schönjahn, M. Bamford, L.A. Donohue, D.B. Lewis, S. Forder, W.-D. Münz, Surf. Coat. Technol. 125 (2000) 66.
[15] Bharat Bhushan, Nanotribology and Nanomechanics an Introduction, second edition, Springer, 2008.
[16] A. Arranz, C. Palacio, Surf. Sci. Spectra 11 (2004) 33.
[17] A. Glaser, S. Surnev, M.G. Ramsey, P. Lazar, J. Redinger, R. Podloucky, F.P. Netzer, Surf. Sci. 601 (2007) 4817.
[18] J.E.B. Randles, Discuss. Faraday Soc. 1 (1947) 11.
[19] S. Surviliene, S. Bellozor, M. Kurtinaitiene, V.A. Safonov, Surf. Coat. Technol. 176 (2004) 193.
[20] D.V. Shtansky, in: A.A. Voevodin, D.V. Shtansky, E.A. Levashov, J.J. Moor (Eds.), Deposition, Characterization, Testing and Application, Ser. II Math. Phys. Chem, 155, Springer, Dodrecht, 2004, p. 155.
[21] V.K. William Harish, C. Barshilia, V. EzhilSelvi, Kalavati, K.S. Rajam, Thin Solid Films 514 (2006) 204.
[22] M. Fenker, M. Balzer, H.A. Jehn, H. Kappl, J.-J. Lee, K.-H. Lee, H.-S. Park, Surf. Coat. Technol. 150 (2002) 101.
[23] E. Söderlund, P. Ljunggren, Surf. Coat. Technol. 110 (1998) 94.
[24] J.C. Caicedo, C. Amaya, G. Cabrera, J. Esteve, W. Aperador, M.E. Gómez, P. Prieto, Thin Solid Films 519 (2011) 6362.
[25] H.A. Jehn, Surf. Coat. Technol. 125 (2000) 212.
[26] V.W. Grips, C.B. Harish, V.E. Selvi, Kalavati, K.S. Rajam, Thin Solid Films 514 (2006) 204.
[27] W. Tato, D. Landolt, J. Electrochem. Soc. 145 (1998) 4173.
[28] Chang Ku-Ling, Chung Shih-Chun, Lai Shih-Hsiang, Han-C. Shih, Appl. Surf. Sci. 23 (6) (2004) 406.
[29] H. Altun, S. Sen, Surf. Coat. Technol. 197 (2005) 193.
[30] J.C. Caicedo, G. Zambrano, W. Aperador, L. Escobar-Alarcon, E. Camps, Appl. Surf. Sci. 258 (2011) 312.